Paper accepted for publication by Applied Acoustics 188 (2022) 108542,
https://doi.org/10.1016/j.apacoust.2021.108542

The distribution of pantograph aerodynamic noise on train external surfaces and the influence of flow

Hui Li, Xiaowan Liu, David Thompson, Giacomo Squicciarini

Institute of Sound and Vibration Research, University of Southampton,
Southampton SO17 1BJ, United Kingdom

Abstract: Aerodynamic noise from the pantograph is significant when a train is running at high speeds and can be important for noise inside the train as well as at the wayside. In this work, the propagation of noise from a pantograph to the train external surfaces is studied, including the influence of the air flow. The noise emitted by the pantograph is modelled using a semi-empirical component-based approach which allows for the main factors of influence. To calculate the distribution of sound on the train external surfaces, the waveguide boundary element (2.5D BE) method is first employed, in which the pantograph is modelled by several equivalent dipole sources. Laboratory experiments are used to verify the 2.5D BE model for predicting the noise around the train due to the pantograph. The pantograph noise is found to be quite localised on the roof directly below the pantograph, where the sound pressure level on the train surface is high, but with increasing distance from the pantograph, it decreases rapidly. Moreover, the difference between the sound pressure level on the train roof and on the sides is about 20 dB in the plane of the pantograph. The influence of flow on the sound propagation is then modelled by introducing the profile of the velocity in the boundary layer into a 2D finite element model using the linearised potential flow model in COMSOL Multiphysics. The air flow causes some amplification in the sound pressure levels in the upstream direction and attenuation in the downstream direction. At high frequency the wind gradient in the boundary layer will change the direction of the sound, leading to the formation of a quiet shadow area in the upstream direction. However, despite these effects, the flow has only a small effect on the region with the highest noise levels beneath the pantograph.

Keywords: pantograph noise, noise propagation, flow influence, boundary layer, 2.5D BE method.

1 Introduction

As the speeds of trains increase, their noise emission becomes an increasing concern, both in the neighbourhood of the line and for the passengers and on-board staff. The aerodynamic noise increases more rapidly with speed than other sources so that, above a certain speed called the transition speed, it becomes the dominant source of noise [1, 2]. Many studies have shown that this transition speed occurs at approximately 300 km/h [3, 4], at least for exterior noise, although it depends on the specific design of train. For interior noise the different transmission paths will affect the relative contributions of the various noise sources but aerodynamic noise is also important here at high speeds. Modern high-speed trains commonly operate at speeds in excess of 300 km/h, at which aerodynamic noise is undoubtedly significant.

The main aerodynamic noise sources identified from different studies on various high-speed trains [5-7] can be classified into two groups. The first consists of the noise generated by flow over structural elements, such as the pantograph and the bogies, as well as cavities, such as the pantograph recess, bogie cavities or inter-coach gaps [8]. These types of source are associated with the surfaces of the structure and cavity flows and the noise has a dipole-like property [9]. The other group of noise sources is generated by turbulent flow, including aerodynamic noise from the turbulent boundary layer surrounding the train and at the rear of the train. This second type of source has a quadrupole-like property [10]. Based on scaling laws [10, 11] the sound power of the dipole-like aeroacoustic sources is proportional to the 6th power of the Mach number while for the quadrupole-like sources it is proportional to the 8th power. The Mach number corresponding to the train speed is much smaller than 1 (for instance, at 300 km/h it is 0.24) suggesting that the quadrupole-like sources may be less important. Additionally, for trains the aerodynamic noise from turbulence is mainly broadband and dominated by low frequencies whereas that from the pantographs and bogies contains tonal components with high pitch (depending on the dimensions) which is more important for the A-weighted sound.

In Japan, the importance of pantograph noise was noticed in the development of the Shinkansen bullet trains [6]. Many experimental studies and efforts have been made to reduce the pantograph noise of high-speed trains since then, including optimisation of the pantograph to achieve low noise radiation [6, 12, 13] and adding noise insulation plates along the sides of the roof [13]. A multi-segment slider was used in the current collector of the low-noise pantographs, contributing to the reduction of the pantograph peak noise levels [13]. Besides, porous

materials [14] and flow control technology [15] have been studied for the reduction of pantograph noise. To identify the relative contributions of each part of the pantograph in terms of their sound power, Grosche and Meier [16] measured the noise from a full-scale DSA pantograph using acoustic mirrors in a wind tunnel. They found that the panhead, the knee joint and the foot region are significant noise sources. Lölgen [17] also measured several types of pantograph in a wind tunnel and identified tonal peaks according to the vortex shedding frequencies expected for different diameters of cylinder.

Latorre Iglesias et al. [18] experimentally studied the noise from individual cylinders, representative of components of a pantograph. In order to gain a better understanding of the aeroacoustic characteristics of the pantograph arms, which are inclined to the airflow, they assessed the dependence of the noise on the yaw angle, flow speed, cross-sectional shape, angle of attack and radiation angle (directivity). They found that the amplitude and frequency of the vortex shedding noise both decrease with increasing yaw angle, whereas the relative bandwidth of the vortex shedding peak was found to increase with the yaw angle for all the cylinder cross-sections considered except for the elliptical cylinders. They also noticed that the cross-sectional shape of the cylinder affects the frequency, amplitude and speed dependence of the vortex shedding noise. A square cylinder was found to be the noisiest and elliptical cylinders the quietest.

Explaining the mechanism of the aerodynamic noise from the pantograph becomes possible after Curle [9] extended Lighthill's acoustical analogy [10] to noise generation in the flow with the presence of stationary solid boundaries. This was later extended to moving surfaces by Ffowcs Williams and Hawkings [19], who showed the existence of monopole and dipole-like noise sources on the structure surfaces. With the development of computing capacity and advanced turbulence models such as the large eddy simulation (LES) [20] and detached eddy simulation (DES) [21], computational aeroacoustics (CAA) became possible using near-field flow information from Computational Fluid Dynamics (CFD) in an acoustic analogy such as the Ffowcs Williams and Hawkings equation. Nevertheless, due to the complexity of the geometry and the flow, it is extremely time consuming to perform detailed aerodynamic noise simulations for a full-scale pantograph. Although Lei et al. [22], for example, have numerically studied a full pantograph in considerable detail, the CFD techniques they used to obtain the noise sources were based on the Reynolds Averaged Navier-Stokes (RANS) model, which is not sufficient to capture the small turbulent structures that are expected to be important for

aerodynamic noise. More recently Kim et al. [23-25] have used a form of DES to model a whole pantograph at reduced scale in combination with a simplified roof cavity. Although good agreement was achieved with wind tunnel measurements for frequencies up to 800 Hz, the model could not take account of small details on the pantograph that are important in generating higher frequency noise.

Liu et al. [26, 27] numerically studied the noise from individual cylinders representing pantograph components. They proposed the idea that by adding spanwise waviness to square bars, the aerodynamic noise can be dramatically reduced. They showed that a straight square bar in cross-flow produces strong tonal noise associated with the vortex shedding. When they introduced waviness along the bar span they found from both numerical simulations and measurements that, when the wave amplitude is nearly half the bar width, a large noise reduction of as much as 30 dB is achieved, including a 10 dB reduction in the broadband level.

To predict aerodynamic noise from complex structures, a semi-empirical component-based approach has been proposed. In this approach, the noise from various components is estimated using normalised spectra that are obtained from experiments or calculations on individual components and are adjusted according to the dimensions and flow conditions of the components. Any flow interactions between components are neglected. The component-based approach was first derived for predicting aircraft landing gear noise [28]. Because it has been found to be effective in practical applications, it was later employed to predict train pantograph noise by Behr et al. [29]. Latorre Iglesias et al. [30] also used this approach to predict the aerodynamic noise of a high-speed train pantograph. They initially used empirical constants obtained from existing noise measurements from full-scale pantographs to calibrate the spectral shape and amplitude for each group of components. A good agreement between the experimental results and the predictions was obtained in terms of overall noise level but the measured spectral shape was governed by individual peaks that were not reproduced by the model. Latorre Iglesias et al. [31] and Liu et al. [32] then developed a more detailed model in which each strut of the pantograph was modelled using existing experimental data for various aerodynamic parameters of cylinders with different cross-sections in an air flow, such as the Strouhal number (i.e. non-dimensional frequency), fluctuating lift coefficient and correlation length. The spectral shape, the effect of the inclination of each of the struts (the yaw angle), and the influence from the cross-section and the incoming flow turbulence intensity, etc. were used to adjust the results for different situations. Based on this, the component-based approach

gives a good agreement with measurements in terms of the sound pressure from a pantograph both from wind tunnel tests and from operational trains. These results showed that the pantograph head was the dominant source of noise.

From the above contributions, the sound emitted by a pantograph can be predicted well using the existing models. However, little attention has been given to the role of pantograph noise in the train interior noise [33], for which it is necessary to understand the propagation of sound from the pantograph to the train external surfaces. Previously, the boundary element method has been adopted to investigate the sound field around a pantograph using a commercial software [22], but in this approach it is difficult to handle high frequencies and large structures. Moreover, the influence of flow on the pantograph sound propagation has not been considered.

Various authors have used numerical methods to consider the influence of flow on acoustic propagation. For example, Bassem et al. [34] developed a simplified two-dimensional BE method with arbitrary uniform mean flow and Zheng and Li [35] used a time domain Eulerian simulation to study acoustic wave propagations with background flow. Meanwhile, Hadi and Iman [36] performed simulations in COMSOL to investigate the sound reduction through a Helmholtz resonator with a background flow. In their studies, the flow field was solved by using CFD, and the acoustics was calculated through a linearised Navier-Stokes equation after a mapping of the flow data. However, these methods are too computationally expensive to apply to the noise on the external surface of a train. An efficient and reliable method for predicting the noise propagation from the pantograph to the train external surfaces is therefore required.

In this work, a wavenumber domain boundary element (2.5D BE) method is employed first to study the noise propagation from the pantograph to the train external surfaces. In this approach the pantograph is replaced by several dipole sources with unit oscillating velocity. The sound power from the pantograph is obtained by using the component-based method and used to determine the source levels, as described in Section 2. The 2.5D BE method and the corresponding numerical models are given in Section 3; comparisons are also shown with laboratory measurements on a scale model. The influence of the flow on the sound propagation is then modelled using a 2D finite element method in COMSOL Multiphysics. The velocity profile in the boundary layer is introduced and the aeroacoustics interface in COMSOL is used to solve the sound propagation in the non-uniform flow. This is explained in Sections 4 and 5.

In Section 6 the results are combined to give an estimate of the noise distribution from the pantograph in the presence of flow. The conclusions are given in Section 7.

2 Sound power of the pantograph

A train pantograph is composed of many different components. The most representative components within a typical pantograph are the contact strips, horns, stroke limiting cage, control rod and pantograph arms, as shown in Figure 1 and detailed in references [30, 37].

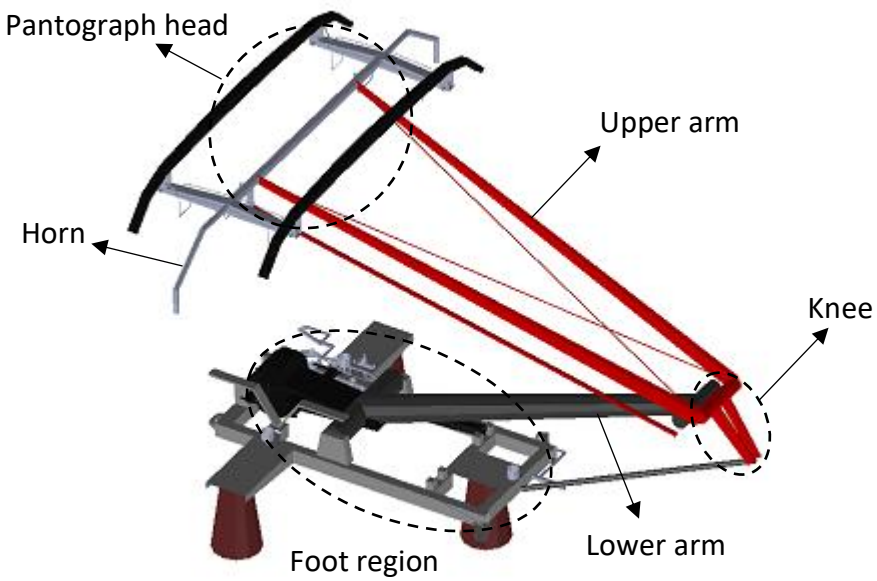

Figure 1. Configuration of the pantograph DSA350, redrawn from [30, 37].

Most of these components can be modelled as cylinders or square bars with different dimensions and different yaw angles towards the flow. The sound radiation from each component is assumed to be the result of the fluctuating dynamic force on the cylinder caused by the interaction of the flow and the structure [11]. In previous research, the aerodynamic noise from single components has been modelled by using CFD [32, 37], taking into account the yaw angle and cross-section shape.

In the prediction of the noise from the whole pantograph, if it is assumed that noise contributions from each component are uncorrelated, and the mean square sound pressure radiated by the whole pantograph can be predicted by the incoherent sum of the spectra of each

individual strut. This is the basis of the component-based approach [31, 32] It is assumed that the pantograph and receiver are both stationary and the flow is moving. This is equivalent to a moving train and moving receiver in stationary air. The mean-square sound pressure in the far field at frequency f due to the pantograph is expressed as [23]

$$\overline{p^2}(f) = (\rho_0 c_0^2)^2 M^6 \sum_i \frac{\eta_i S_i F_i(f)}{R_i^2} \frac{D_{\mathrm{rad},i}(\psi, \phi)}{(1 - M\cos\theta)^4} \tag{1}$$

where the subscript *i* refers to each strut, *M* is the Mach number, S_i is the total surface area of each component of the pantograph. $F_i(f)$ is a normalized spectrum obtained using empirical relations. As each component has a dipole property, the directivity factor should be included in this case. $D_{\mathrm{rad},i}(\psi, \phi)$ is the directivity of the noise radiated by each strut, depends on the angle between the axis of the fluctuating lift force (perpendicular to the flow direction) and the receiver position in the azimuthal plane (ψ) and in the elevation plane relative to the azimuthal plane (ϕ). Frame of coordinates and the angles ϕ and ψ are defined as shown in Figure 2.

The directivity function for a theoretical dipole source is used for the peak noise at the vortex shedding frequency while the broadband noise is assumed to be omnidirectional [30]. The distance *R* between the cylinder and the receiver is defined separately for each cylinder. The Doppler factor $D^4 = (1 - M\cos\theta)^4$ accounts for the effect of the convective amplification for a dipole source, depending on the observer position, where θ is the angle between the direction of the flow and the observer position (Figure 2). η_i is the amplitude factor, given by

$$\eta = \frac{St^2 C_{l,\mathrm{rms}}^2 L l_c d}{16S} \tag{2}$$

where St is the Strouhal number related to oscillating flow mechanisms, defined by $St = fd/U$ (*f* is the frequency of vortex shedding, *d* is the cylinder diameter and *U* is the flow velocity), $C_{l,\mathrm{rms}}$ is the root mean square (rms) fluctuating lift coefficient, (the lift coefficient $C_l = F_l/(0.5\rho U^2 dL)$ with F_l being the lift force). *L* is the length of the cylinders, l_c is the spanwise correlation length, normalised by the cylinder diameter, d. Each component of the pantograph is modelled independently by choosing an appropriate normalized spectrum $F_i(f)$. This allows prediction of the far-field noise spectrum based on empirical databases of *St*, $C_{l,\mathrm{rms}}$ for different cases of cylinders, rather than relying only on measurements or simulations of

noise. The normalized spectrum, $F_i(f)$, is determined in different ways for peak and broadband noise [31, 32].

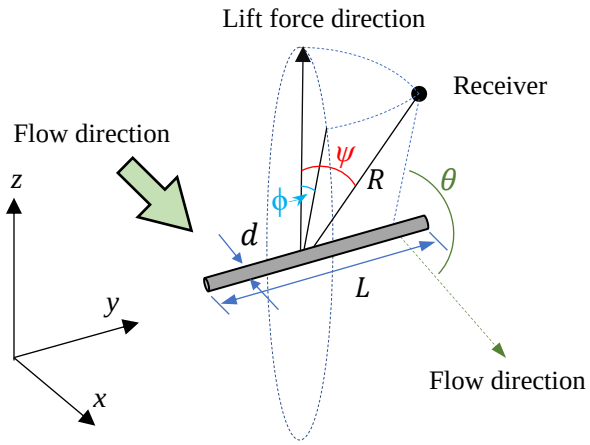

Figure 2. Definition of coordinates and the angles ϕ and ψ in relation to the direction of the fluctuating lift force, redrawn from [30].

From this model, the total sound power level from the pantograph can be determined by integrating the sound pressure level over a surface in the far field by assuming a compact source radiating in free space. Figure 3 shows the total sound power from the pantograph DSA350 at train speed 290 km/h and the contributions from the head, the horns, the upper and lower arms.

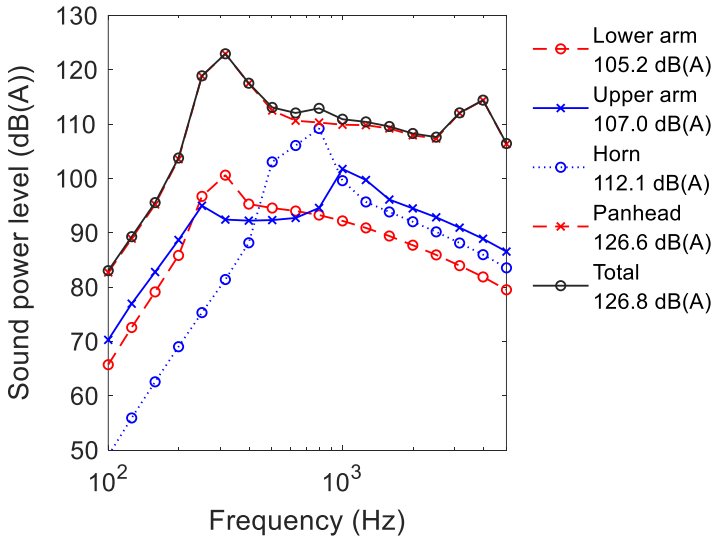

Figure 3. Predicted sound power (A-weighted) from the pantograph and contributions from each part, 290 km/h.

From Figure 3, it can be seen that most of the sound power is due to the pantograph head. It has a spectral peak at about 200 Hz, due to the contact strips within the head. There is another peak at 4000 Hz in the spectrum of the pantograph head, due to components with very small radius. The upper and lower arms radiate less noise because they are yawed to the flow. The horn is not yawed but it has a smaller radiating surface than the head. Nevertheless, due to its directivity the horn is important for wayside noise [32].

3. Modelling pantograph noise propagation

3.1 The 2.5D BE method

If the geometry of the problem can be considered uniform and of infinite length in one direction, e.g. x, the acoustic boundary integral equation can be conveniently solved in the 2D domain for a range of wavenumbers in the x direction. This can be achieved through a 2.5D formulation where pressure, velocity and the Green's function are expressed as functions of k_x, y and z and the boundary integrals are solved over the perimeter of the boundary region Γ. The wavenumber domain integral equation therefore becomes [38]

$$\tilde{p}(k_x, y', z') = -\int_{\Gamma} \left(\mathrm{i}\rho\omega \tilde{v}(k_x, y, z)\tilde{\psi}(k_x, y, z|y', z') + \tilde{p}(k_x, y, z)\frac{\partial \tilde{\psi}(k_x, y, z|y', z')}{\partial n} \right) \mathrm{d}\Gamma \tag{3}$$

where the tilde indicates quantities in the wavenumber domain. $\tilde{v}(k_x, y, z)$ in Eq. (3) is the particle velocity in the wavenumber domain normal to the surface, which is calculated by applying the Fourier transform to the normal velocity in the spatial domain:

$$\tilde{v}(k_x, y, z) = \int_{-\infty}^{\infty} v(x, y, z) e^{\mathrm{i}k_x x}\, \mathrm{d}x \tag{4}$$

In Eq. (3) the wavenumber in the *x* direction, k_x, is independent of *y*, *z* and the Green's function $\tilde{\psi}(k_x, y, z|y', z')$ takes the same form as the 2D fundamental solution [39]

$$\tilde{\psi}(k_x, y, z|y', z') = -\mathrm{i}\frac{1}{4} H_0^{(2)}\left(\sqrt{k_0^2 - k_x^2}\, r\right) \tag{5}$$

with $H_0^{(2)}$ being the Hankel function of the second kind and zero order, and k_0 the wavenumber in air. If $k_x > k_0$, the wavenumber in the 2D domain is imaginary, and the sound waves will decay exponentially with distance in the *y*–*z* plane. The spatial distribution of sound pressure can be calculated by an inverse Fourier transform

$$p(x,y,z) = \frac{1}{2\pi}\int_{-\infty}^{\infty} \tilde{p}(k_x,y,z)\, e^{-\mathrm{i}k_x x}\mathrm{d}k_x \tag{6}$$

3.2 Numerical model for the pantograph noise propagation

A 2.5D BE model is used to model the noise propagation from the pantograph to the train external surfaces. The train is represented by its cross-section. However, it needs to be noticed that the pantograph is a distributed source. Whether it can be treated as a compact source depends on the source dimension, the relative distance from the source to the receiver and the frequency. If the pantograph is subdivided into several segments, each segment has a relatively small dimension compared with the distance from the source to the train external surfaces, and thus, they will roughly meet the geometrical far field assumption. The distance from the pantograph head to the train roof is estimated as 1.4 m from its configuration in [37], and the sound power of the pantograph is concentrated above 200 Hz when the train speed is 290 km/h, which can roughly meet the acoustical far field condition ($kr >> 1$). The pantograph is therefore regarded as an array of dipole sources according to the directivity of the various components. The method to introduce a point dipole source in the 2.5D BE model is described in [38].

The pantograph is sub-divided into the panhead, the arms, and the horn, and each of them is modelled by using several dipole sources. The locations and number of the dipoles should be chosen based on the correlation length of the components and the frequency; moreover, the direction of the dipole should be consistent with the expected directivity of the source, see Figure 4(a). The final 2.5D models are indicated in Figure 4(b). Five dipole sources are used to model the pantograph head, two inclined at 45° are used to model the horn and another two horizontal dipoles are used to model the upper arms. Their relative locations are listed in Table 1. The knee and the foot parts of the pantograph are located in the boundary layer and their contributions to the total sound power are small compared with the pantograph head, as can be seen from Figure 3. Besides, Zhang et al. [40] compared with the contributions of different parts to the overall noise level of a similar pantograph and found the most important noise

sources are located at the pantograph head region. The lower arms and the foot region produce about 15 dB(A) less, and the knee about 20 dB(A) less than the pantograph head. Therefore, the knee and the foot parts are omitted from the model. The various sources are assumed to be incoherent, so they are created in separate 2.5D BE models. A typical train cross-section is included in the model with the roof of the train about 4 m above the ground.

Linear boundary elements with length 0.01 m are used to represent the train cross-section. Each dipole source is represented by a circle in the 2.5D models [38]. The radii of the sources are 0.005 m, which is small enough for the region away from source (in the *x*-direction) to have negligible effect on the radiated sound. 36 elements are used for each source. The boundary condition on the sources is given by a unit oscillating velocity from which the corresponding normal velocity is determined. The oscillating direction is along the axis of the dipole. The sound power of each part of the pantograph obtained from the component-based approach is used to adjust the source levels. For this exterior problem, 'CHIEF' points are introduced inside the train body to avoid the non-uniqueness problem [41].

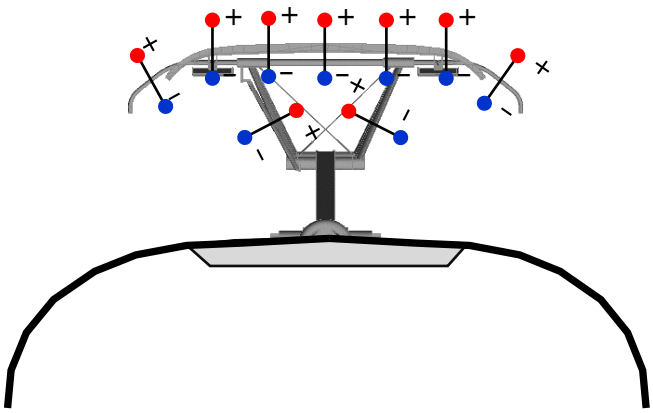

(a)

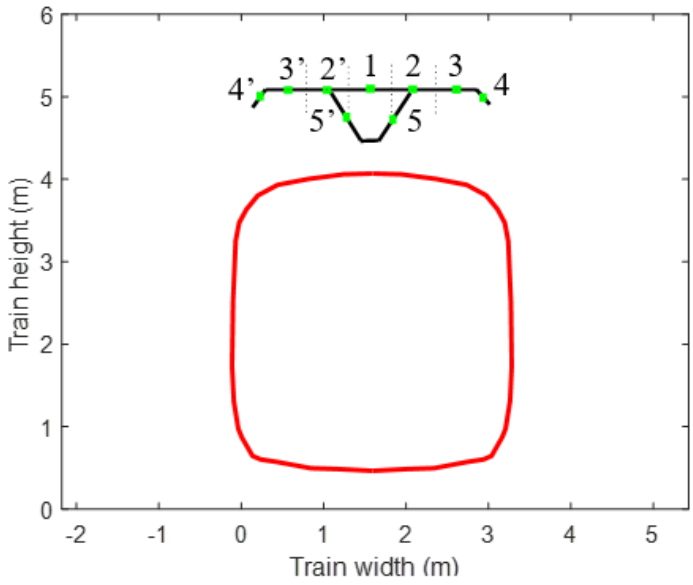

(b)

Figure 4. (a) Pantograph on train roof showing location of equivalent sources on the pantograph head; the foot region of the pantograph is located in the recess. (b) The 2.5D model for pantograph noise, including a typical train cross-section.

Table 1. Locations of the dipole sources above the train roof. Height (z) is measured relative to the ground.

Points	Location (y, z), m	Orientation	Part of
1	(0, 5.4)	Vertical	Head
2 and 2'	($\pm$0.271, 5.4)	Vertical	Head
3 and 3'	($\pm$0.542, 5.4)	Vertical	Head
4 and 4'	($\pm$0.808, 5.27)	Inclined at 45^o	Horn
5 and 5'	($\pm$0.280, 5.08)	Lateral	Upper arm

3.3 Sound pressure on the train external surfaces

The pantograph is assumed to be symmetrical about the train centreline. The noise from point sources 1-5 is calculated on the train external surfaces and the others are obtained by symmetry. Figure 5 shows the sound pressure on the train external surfaces in the spatial domain due to point sources 1, 3, 4 and 5 with unit oscillating velocity (at 200 Hz).

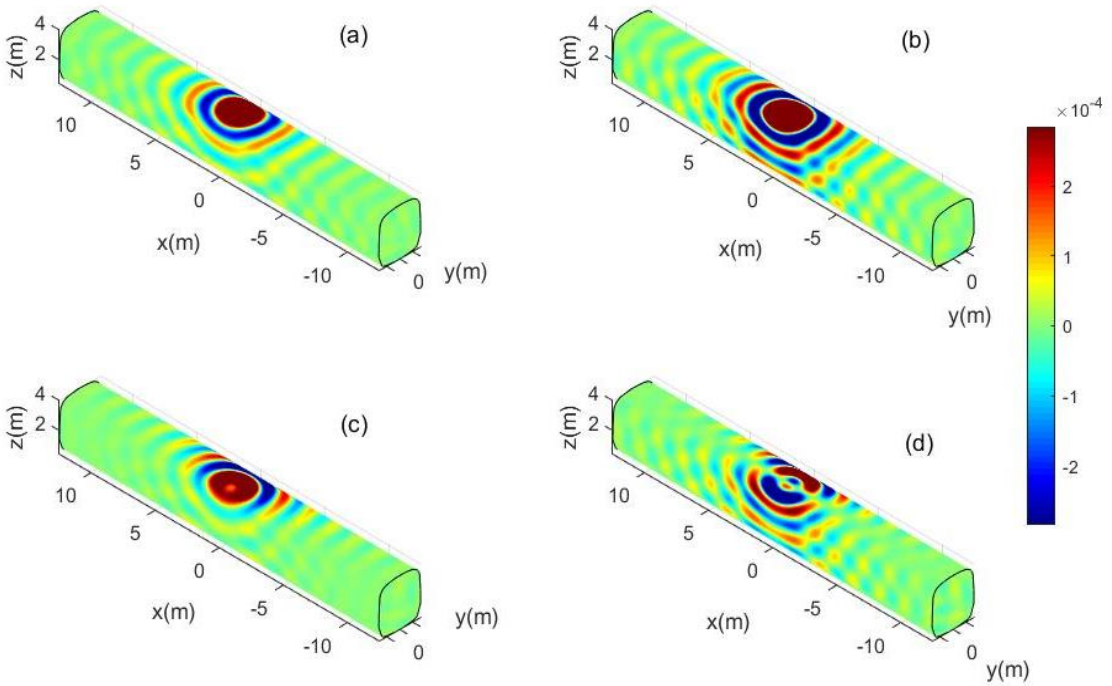

Figure 5. Real part of the sound pressure (Pa) on the train external surfaces due to dipoles with unit oscillating velocity (at 200 Hz). (a) From point source 1, a vertical dipole located in the middle of the contact strip, (b) from point source 3, a vertical dipole close to one end of the contact strip, (c) from point source 4, a dipole inclined at 45^{o} to the vertical direction for the horn (d) from point source 5, a lateral dipole for the upper arm.

A scale factor is used to adjust the sound pressure obtained from the 2.5D prediction to correspond to the actual source strengths obtained from the component-based model. The adjustment is performed based on the following relation:

$$\overline{p^2} = \sum_{m=1}^{3} \sum_{k=1}^{n} \overline{p_{\mathrm{k}}^2} \frac{\mathrm{W}_m}{n\mathrm{W}_{\mathrm{d}}} \tag{7}$$

where the three important parts considered, the panhead, the horn and the upper arms, are denoted by m = 1, 2, 3. W_m is the sound power from the m^{th} part of the pantograph calculated from the component-based approach. Each part is replaced by n dipoles, specifically, five for the head, and two each for the horn and the upper arms. W_{d} is the sound power of a single dipole source in the 2.5D models (in which a unit oscillating velocity is used). $\overline{p_{\mathrm{k}}^2}$ is the mean square pressure on the train external surfaces calculated from the 2.5D BE model due to the k^{th}

dipole which has a unit oscillating velocity and $\overline{p^2}$ refers to the actual mean square pressure on the train external surfaces due to the pantograph.

The total sound pressure level distribution on the train external surfaces due to the contributions from all three parts is calculated by adding their mean square pressures together. Figure 6(a) gives the A-weighted sound pressure level on the train external surfaces in the 500 Hz one-third octave band and Figure 6(b) gives the overall A-weighted sound pressure level. The sound pressure levels ahead of the pantograph and behind it are the same, as the convective effect is ignored here.

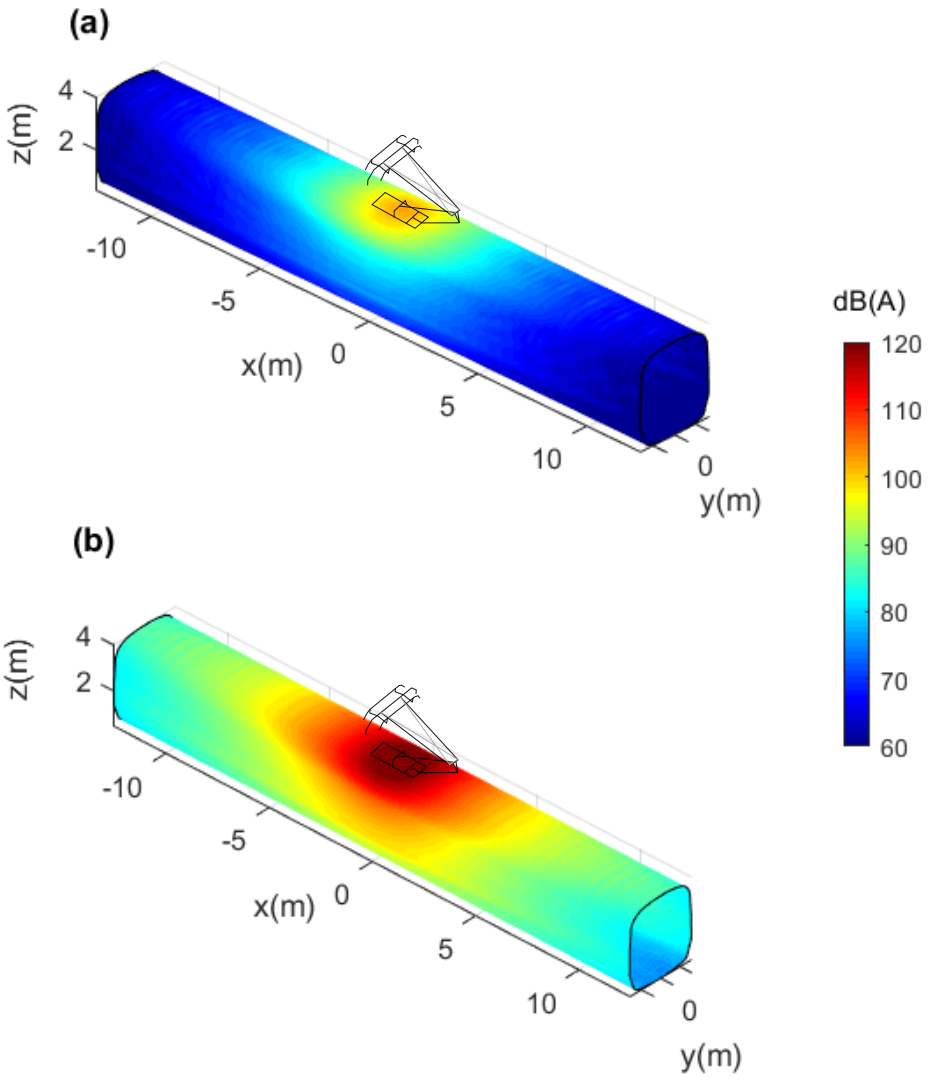

Figure 6. A-weighted sound pressure level on the train external surfaces due to a pantograph at 290 km/h, (a) 500 Hz one-third octave frequency band, (b) overall sound pressure level. dB(A), re 2×10^{-5} Pa.

3.4 Comparison with measurements

To validate the prediction of the sound distribution on the train external surfaces, laboratory measurements were performed in the anechoic chamber at the University of Southampton. A 1:5 scale simplified car body, made of a dense foam which was sealed with varnish, was set up above a 1:5 scale track using wooden supports [42]; the track and the car body were not in contact. The track model is 2 m long and 0.8 m wide, and the train is 2.5 m long, 0.56 m wide and 0.45 m tall. The distance from the top of the sleepers to the train floor was about 0.23 m.

The track and ballast are not essential in these measurements, but they can provide more representative absorptive properties below the train. A sound source was used that consists of a driver connected to a stiff tube with a nozzle of diameter 1.5 cm. The sound emitted from the tube is approximately omnidirectional and has a volume velocity that is independent of the source location. This arrangement allows the source to be placed at a precise location within the model. The source was excited with white noise, although the sound emitted is modified by the acoustic properties of the tube.

The source nozzle was located 0.24 m above the train roof in the middle of the train cross-section and the sound pressure distribution around the train body was measured, see Figure 7(a). The source nozzle gives a monopole-like sound distribution, rather than a dipole source, but if the 2.5D model can predict the sound distribution on the scaled train model due to a monopole source above it, it can also be trusted to predict the sound pressure from a dipole source. Microphones were located along the centrelines of the train roof and one side surface. On each surface, there were 11 measurement locations between the middle of the carriage and one of its ends, with a spacing of 0.1 m.

Figure 7(b) shows the corresponding numerical model. The train and track (ballast box) are modelled by linear boundary elements with element size 0.01 m (allowing the calculation to be carried out up to 5 kHz based on six elements per wavelength). The boundary condition of the train surface is set as rigid while for the ballast an acoustic impedance boundary condition is given to the top surface and the sides are rigid. The source in the numerical model is represented by a circle with radius 0.005 m and 36 boundary elements [38]. The source strength (volume velocity) is derived from the sound power of the source used in the measurement. Five 'CHIEF' points are added inside the train and three are used in the ballast box to avoid the non-uniqueness problem for exterior problems. The measured locations are illustrated as points P1, P2 in the corresponding numerical model, as shown in Figure 7(b).

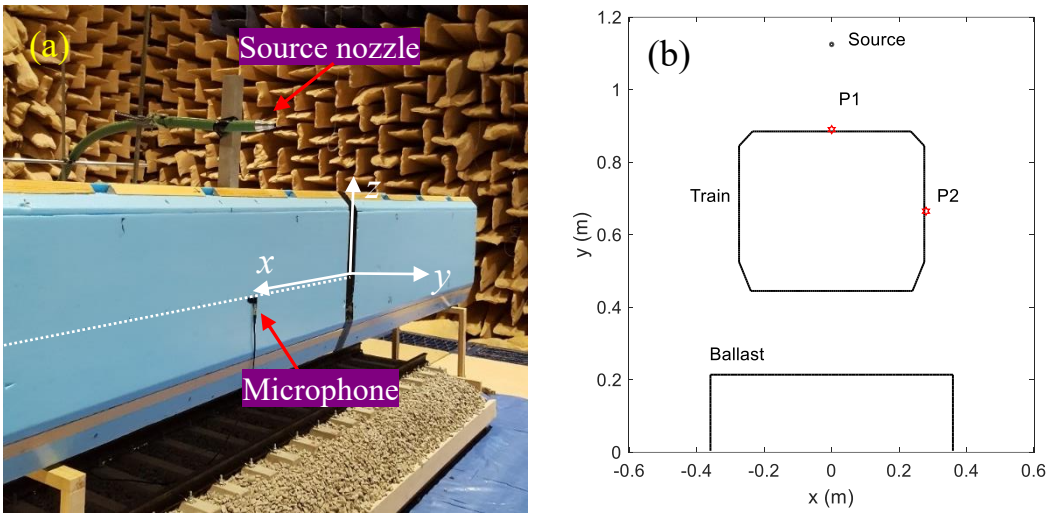

Figure 7. (a) Model train body used in the measurement, (b) the corresponding 2.5D BE model.

The predictions and the measurements are compared in one-third octave bands between 1.25 kHz and 5 kHz (250 to 1000 Hz at full scale). In the predictions, the results at five frequencies in each one-third octave band are averaged. The comparisons are shown in Figure 8 for four example frequency bands. The predictions agree well with the measurements. These results show that the sound pressure level on the train roof decays with distance faster than that on the side, and directly below the source the sound pressure level on the roof is about 20 dB higher than that on the side.

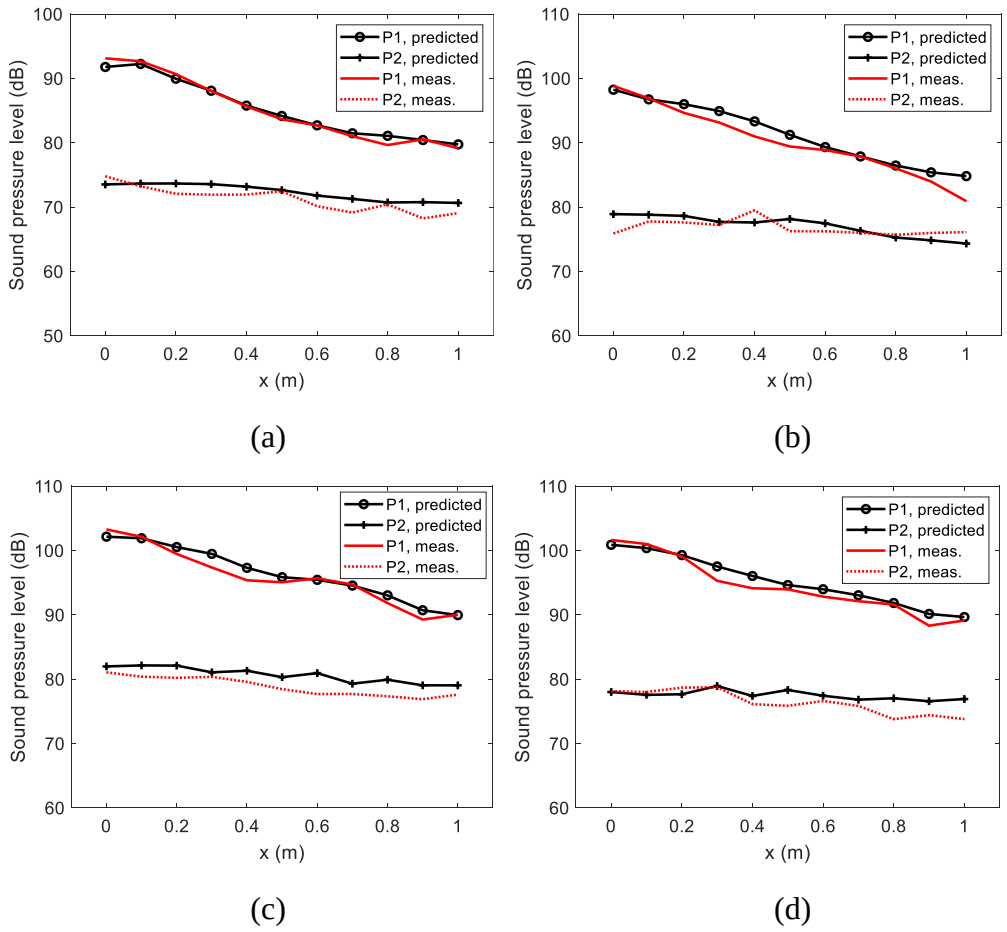

Figure 8. Comparison between predictions and measurements on scale model train. (a) 1250 Hz, (b) 2000 Hz, (c) 3150 Hz, (d) 5000 Hz.

4. Boundary layer on train external surface

In reality, the pantograph is moving with the train, and the sound propagation from the pantograph should therefore be considered as a moving source in a largely static medium. However, it is easier to consider it as a stationary source in a wind that is flowing in the opposite direction. Because of the viscosity of the air and the presence of the train surfaces, a turbulent boundary layer is generated around the train when it runs at high speeds. Detailed measurements on the boundary layer development over the roof of a train are limited in the literature. A short series of measurements were made above a scale model four-car ICE2 train in [43] but the scale effects and the lack of realistic roof roughness inherent in those measurements make the results difficult to interpret. For simplicity, the theory of flow over a flat plate is adopted in this work to approximate the boundary layer. In terms of the Reynolds number $Re = \rho U x/\mu$, where x is the length scale and μ is the fluid viscosity, when $Re >$

5×10^5 the flow becomes unstable and transition to a turbulent boundary layer occurs [44]. The mean velocity profile in the boundary layer can then be described by a power law [44],

$$\overline{U}_1 = U\left(\frac{Z}{\delta}\right)^{\frac{1}{7}} \tag{8}$$

where U is the train speed, z is the distance from the train surface in its normal direction, δ is the thickness of the turbulent boundary layer which grows with x according to [44] as

$$\delta \simeq 0.37x\, Re^{-1/5} \tag{9}$$

The thickness δ thus varies with x along the train axis direction. For the boundary layer on the train roof, x is the distance from the front of the train to the location of the pantograph. The inter-coach gaps are narrow and so it is assumed that they will not greatly affect the growing trend of the boundary layer thickness. Although the detailed designs of high-speed trains vary, for a typical high-speed train with eight carriages, there are generally two pantographs mounted on the train roof: one is near the front at typically about 40 m from the front of the train, the other is nearer the rear at about 160 m from the front. If the train runs at 80 m/s (290 km/h), the corresponding Reynolds numbers at the two pantograph positions are 2.1×10^8 and 8.5×10^8, indicating that the flow is fully developed into turbulence. Therefore, the above expressions for the boundary layer thickness and mean velocity profile in the turbulent boundary layer will be used.

The thickness of the boundary layer at these two positions can be calculated from Eq. (9) by applying these different values of *x*. This work focuses on the pantograph at 40 m from the front of the train for a train speed of 80 m/s (about 290 km/h), which leads to a turbulent boundary layer thickness of about 0.35 m. Substituting this thickness into Eq. (8), the mean velocity profile in the turbulent boundary layer can be estimated. Figure 9 shows the estimated thickness of the boundary layer when the train runs at 80 m/s; the velocity profiles at the positions 40 m and 160 m from the front of the train are also shown. This indicates how the thickness of the boundary layer increases with increasing distance from the front of the train and how the velocity profiles varies.

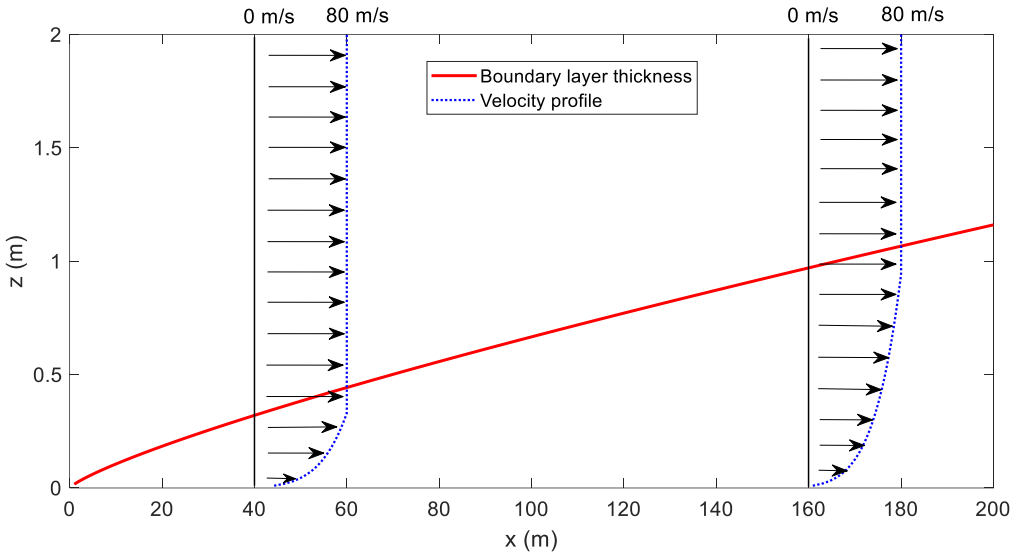

Figure 9. Thickness of the turbulent boundary layer and the velocity profile at 40 m and 160 m from the front of the train for a train speed of 80 m/s (about 290 km/h).

5 Sound propagation in velocity boundary layer

For sound propagation in a uniform mean flow, there is an analytical solution to calculate the sound pressure [11]. For an external force source term associated with aerodynamic noise, the convective effect on sound pressure amplitude is described by $1/D^2$ (see Eq. (1) which is expressed in terms of squared pressure), where $D = 1 - M\cos\theta$ is the Doppler factor [11]. However, the influence of the gradient flow in the boundary layer attached to the train external surface on the noise transmission is more difficult to model by using theoretical analysis. Moreover, the 2.5D BE model is not suitable for this analysis.

An alternative approach is to introduce the velocity distribution including the boundary layer into a finite element model of the sound propagation through the moving medium. COMSOL Multiphysics is employed in this work. The aeroacoustics interface with linearized potential flow in the frequency domain in COMSOL can calculate the sound propagation in uniform or non-uniform flow [45]. This is available for both 2D and 3D problems but, considering the size of the domain above a train roof, a 3D FE model is computationally very expensive at high frequencies. Considering that the flow influence, $1/D^2$, is the same for 2D and 3D problems, and the relative difference caused by the flow in the sound distribution on the train external surface is of more interest than the absolute values, a 2D FE model is created in the vertical plane along the train axis direction (the *x*-*z* plane), which is shown in Figure 10 below. The

background flow is introduced based on the simplified analysis of Section 4; turbulence is neglected but it is expected that the main effects due to the mean flow will be captured correctly.

In the FE model, the 2D acoustic domain extends from x = -15 m to x = 15 m in the train axis direction and from z = (0, 3) m in the vertical direction with z = 0 m at the train roof. Outside the acoustic domain there is a perfectly matched layer (PML). The thickness of the PML is 2 m and its parameters are set according to ref. [46] in order to avoid sound reflection at its outer boundary. A vertical dipole source is created in the acoustic domain at (x, z) = (0, 1.4) m. The dipole source is represented by a small circle (radius 0.01 m) with unit fluctuating velocity in the vertical direction according to ref. [38]. To model the convective effect, the velocity field including the boundary layer is added as a background flow field in the COMSOL model. The location-dependent velocity profile of the flow from Figure 9 (corresponding to the pantograph at x = 40 m) is used, with a maximum flow speed of 80 m/s.

The acoustic domain and the PML are meshed with rectangular elements, the size of which is chosen to ensure at least six elements per wavelength at 3150 Hz. The flow velocity changes rapidly in the boundary layer, so therefore an increased mesh density is used in the boundary layer. In the vertical direction the element size increases from 1 mm at the roof to 20 mm above the boundary layer, whereas in the train axis direction the element size is uniform at 10 mm. This was chosen based on a mesh convergence study that was carried out, in which the mesh was refined until the results did not change with further improvement of the mesh.

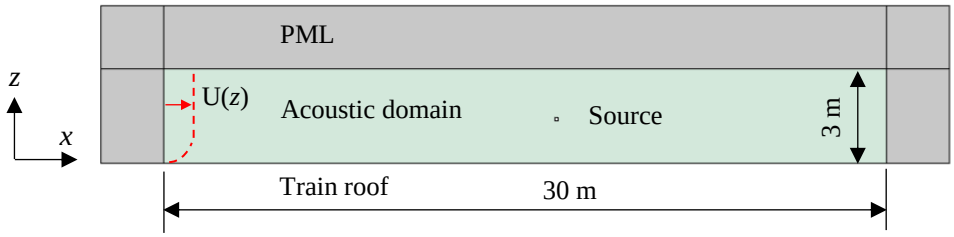

Figure 10. Schematic view of the COMSOL model for sound propagation in non-uniform flow.

The influence of the gradient flow in the boundary layer on the sound propagation is frequency dependent. The sound field in the vertical plane above the train roof at two example frequencies, 200 Hz and 1600 Hz, is given in Figure 11. From Figure 11(a), it can be noticed that when

sound propagates in the flow, the apparent movement of the wave front is the combination of the acoustic propagation and the convective effect of the mean flow: in the upstream direction, the acoustic propagation and the convective effect cancel each other to some extent, and in the downstream direction the two effects add up. As a result, the apparent acoustic wavelengths in the upstream direction are compressed and those in the downstream direction are stretched.

A similar effect can be noticed in Figure 11(b). In addition, however, a shadow area is formed in the upstream direction close to the train surface. This occurs because, in the upstream direction, the velocity gradient within the boundary layer causes the sound to refract away from the train roof. Within a particular range of incident angles, the velocity boundary will make the sound fully reflect before it reaches the roof [47]. The shadow area is not found at 200 Hz because the acoustic wavelength is much larger than the thickness of the velocity boundary layer (about 0.35 m), so the refraction of sound caused by the boundary layer is not significant. In the downstream direction the velocity gradient refracts the sound towards the roof, and the sound can always reach the train roof for all incident angles and frequencies. There is therefore no shadow area in the downstream direction.

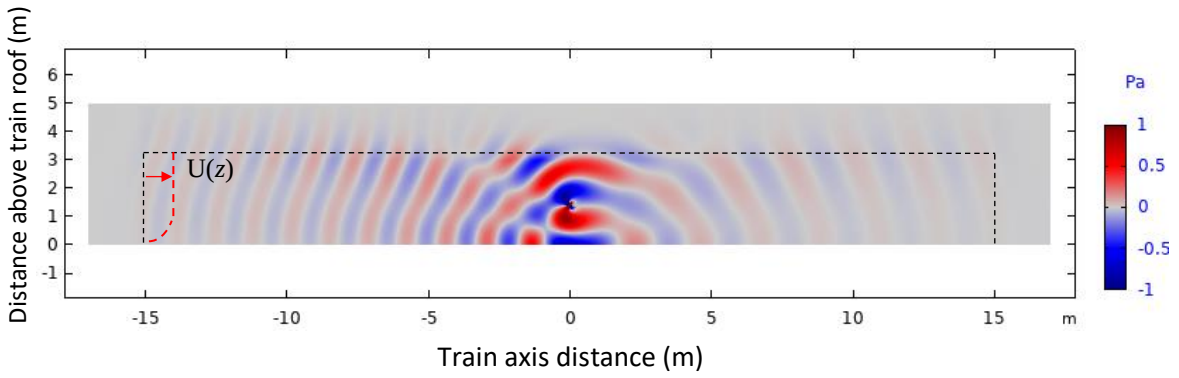

(a)

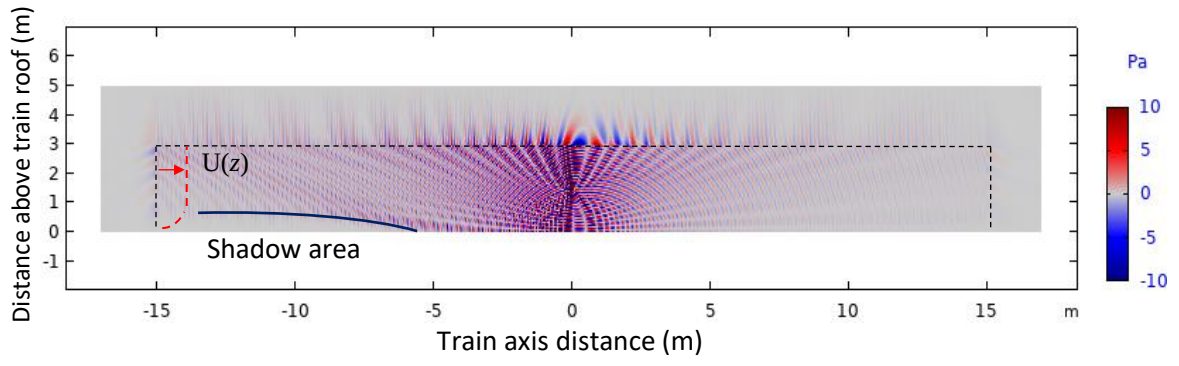

(b)

Figure 11. Real part of the sound field in the vertical plane (x-z plane) subject to a boundary layer flow at maximum flow speed 80 m/s. (a) 200 Hz, (b) 1600 Hz.

The sound pressure level (SPL) on the train roof along the train centreline obtained from the COMSOL model is plotted for different frequencies in Figure 12; these results are normalised to the same value at $x = 0$. It is clear that, in the downstream direction, the influence of the flow on the sound propagation is quite similar at different frequencies, while in the upstream direction, the flow influence depends strongly on frequency. The flow affects the sound pressure in the upstream direction in two different ways: the convective effect due to the flow increases the SPL while the velocity gradient in the boundary layer refracts the sound away from the train roof, which decreases the SPL.

There is a critical frequency at around 800 Hz where the acoustic wavelength is close to the thickness of the velocity boundary layer. Above this frequency, a relatively quiet area appears in the upstream direction. With increasing frequency, the critical point (where the full reflection occurs) moves towards $x = 0$ and it gradually converges at around $x = -4$ m. At 315 Hz and below, the acoustic wavelengths are much greater than the thickness of the boundary layer, and the velocity gradient in the boundary layer does not affect the sound propagation significantly. Thus, no quiet area is found in the upstream region for these frequencies. Between 315 Hz and 800 Hz, a transition region occurs.

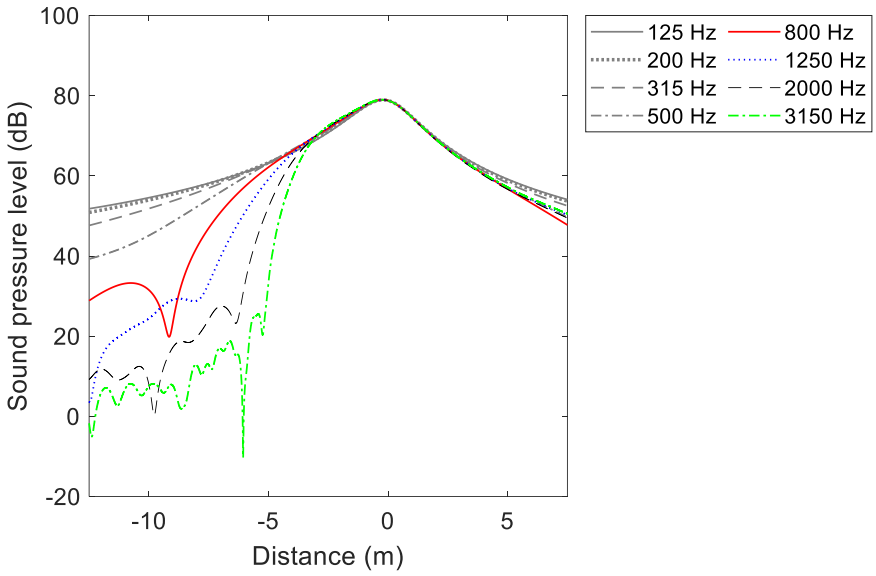

Figure 12. SPL on the train roof at different frequencies for maximum flow speed 80 m/s, normalised to the same value at $x = 0$.

Figure 13 compares the SPL on the train roof at three example frequencies between the cases with and without the flow influence. From this, it can be concluded that the flow causes an attenuation in the SPL in the downstream direction for all the frequencies although the attenuation is greater at higher frequencies. The influence of the flow on the sound propagation in the upstream direction is more complex. At low frequencies, for example at 200 Hz shown in Figure 13(a), the velocity gradient in the boundary layer has little influence on the sound transmission, and the flow influence can be modelled by a uniform flow, shown for comparison. At high frequency, for example at 1600 Hz shown in Figure 13(c), the velocity gradient in the boundary layer has a large influence on the sound transmission in the upstream direction. For $x < -4$ m, there is a large drop in the SPL, which is due to the full reflection of sound by the velocity boundary layer. Between $x = (-4, 0)$ m, where the full reflection does not happen, the SPL shows an increase relative to the case without flow due to convective amplification. In the intermediate frequency range, for example at 500 Hz shown in Figure 13(b), the SPL increases first in the upstream direction. Then, even though there is no sudden drop, the SPL decreases more quickly for $x < -5$ m.

For all frequencies, the sound pressure on the train roof is quite localised directly below the pantograph, with the sound decaying by 10 dB from its maximum value by 4 m upstream and

3 m downstream. In this region where the SPL on the roof is highest, the flow has little effect on the sound propagation (0.9-1.2 dB difference in SPL).

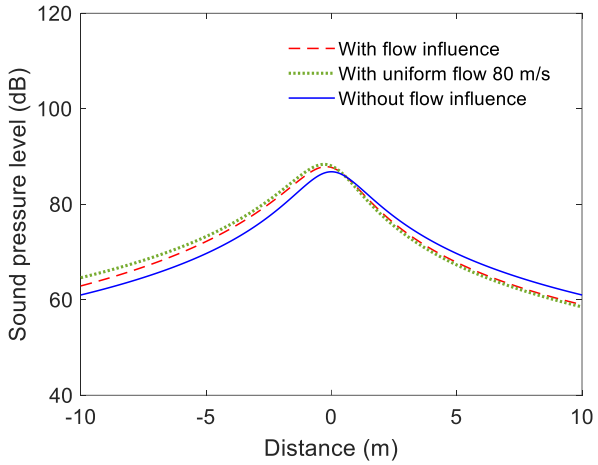

(a)

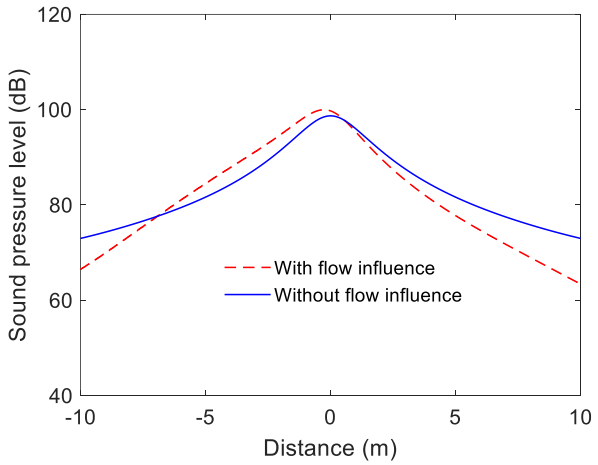

(b)

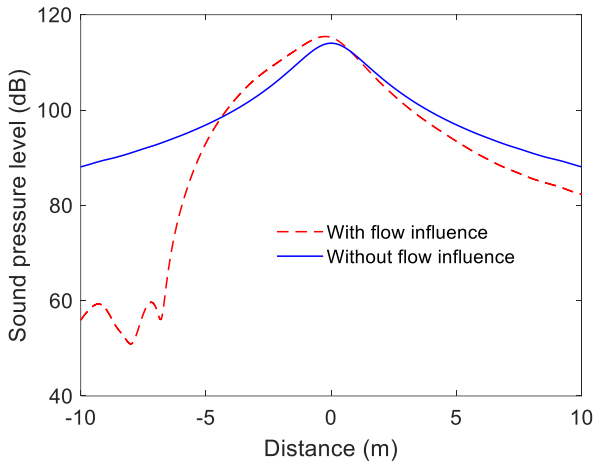

(c)

Figure 13. Comparison of SPL on the train roof at three example frequencies. (a) 200 Hz, (b) 500 Hz, (c) 1600 Hz.

6 Sound pressure level on the train external surfaces in flow

Finally, the various results are combined to give an estimate of the pantograph noise on the train surface including the influence of flow. At each frequency the difference between the SPL of the two cases, with flow and without flow, calculated using the 2D FE model in Section 5, is used to adjust the results obtained from the 2.5D BE model in Section 3. This is done by calculating the SPL on the train external surfaces in each 1/3 octave band using the 2.5D BE method and adding the difference in dB caused by the flow for the corresponding value of x. The SPL on the train external surfaces caused by the pantograph when the train is running at 290 km/h is calculated by summing the corresponding mean square sound pressure in each one-third octave band. As stated before, the pantograph located on the second coach, 40 m from the front of the train is considered. The corresponding overall A-weighted sound pressure on the train external surfaces due to this pantograph at 290 km/h is shown in Figure 14. In comparison with Figure 6, the sound pressure in the upstream direction is higher and that in the downstream direction is lower. The amplification and attenuation are caused by the convective effect of the flow and they depend on the train speed.

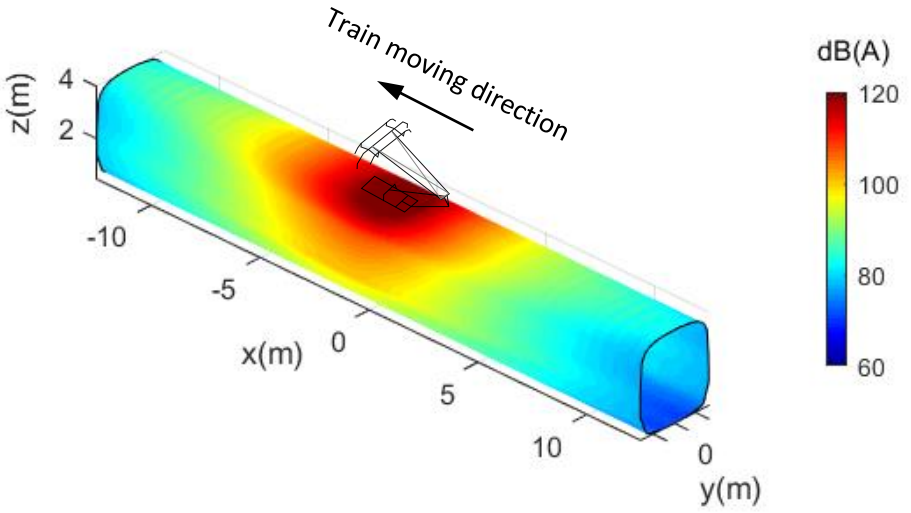

Figure 14. Overall A-weighted sound pressure level on the train external surfaces due to the pantograph including the influence of flow; train speed 290 km/h.

To show these results quantitatively, the overall A-weighted SPL on the train roof along the centreline is plotted in Figure 15 and compared with the case in which the influence of flow is ignored. The flow convective effect increases the SPL on the train roof surface in the first 7 m in the upstream direction. At larger distances in the upstream direction, the level drops due to the sound refraction by the boundary layer. In the downstream direction, the flow influence decreases the SPL and the reduction is about 4 dB at 10 m from the pantograph.

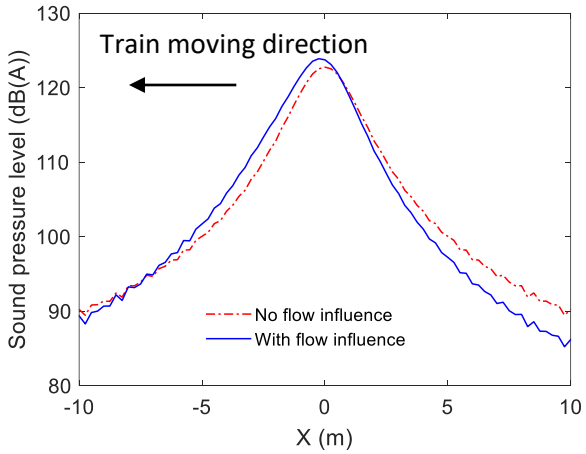

Figure 15. Overall A-weighted sound pressure level from the pantograph on the train roof along the centreline at 290 km/h.

6 Conclusions

The noise propagation from a pantograph to the train external surfaces has been studied by replacing the pantograph by several dipole sources and modelling the sound propagation by using the 2.5D BE method. The sound power from the pantograph is calculated from the component-based approach and this is used to adjust the source level in the 2.5D BE model. Laboratory measurements on a scale model train are used to validate the 2.5D model. The simulation on the scale model train shows that the difference between the sound pressure level on the train roof and on the sides is about 20 dB in the plane of the pantograph. The levels gradually converge with increasing distance and there is about 10 dB difference at a distance of 1 m for the scale train model (5 m for full scale). The measurements show a very similar trend. The sound pressure on the full train external surfaces from the 2.5D model shows that the pantograph noise is quite localised on the roof directly below the pantograph, where the sound pressure level on the train surface is high, but it decreases rapidly with increasing distance from the pantograph.

The flow will cause amplification in the sound pressure levels in the upstream direction and attenuation in the downstream direction. Besides, the velocity gradient in the boundary layer will change the direction of the sound, thus making the sound refract away from the train surfaces in the upstream direction and towards the train surfaces in the downstream direction. The influence of flow on the noise propagation is different at low and high frequencies. At low frequency, where the sound wavelength is larger than the thickness of the turbulent boundary layer, the boundary layer can be ignored, and the wind can be simply considered as a mean flow. However, at high frequency, the boundary layer profile has a great influence on the sound propagation in the upstream direction. A quiet shadow area is formed in the upstream direction at some distance away from the source. The simulations show that the sound pressure level on the train external surfaces in the downstream direction will decrease by about 4 dB at 10 m distance while in the upstream direction it will first increase and then, after around 5 m from the pantograph location, the sound pressure level will reduce more rapidly due to the sound refraction at high frequencies. As experimental validation of the influence of flow has not been possible in the present study, it is recommended that measurements of sound on the train roof

surface, e.g. using flush-mounted microphones, should be used for comparison with the results of this study.

Acknowledgements

The work presented in this paper has received funding from China Scholarship Council. The authors want to acknowledge Laimonas Ratkevicius and Ben Lawrence who built the scale train and track models in their MSc and BEng projects, also special thanks to Dr. Hongseok Jeong for helping in the laboratory measurements. Data published in this paper are openly available from the University of Southampton repository at https://doi.org/10.5258/SOTON/D2033.

References

1. D.J. Thompson, Railway noise and vibration: mechanisms, modelling and means of control, Elsevier, 2008.
2. D.J. Thompson, E. Latorre Iglesias, X.Liu, J. Zhu, and Z. Hu, Recent developments in the prediction and control of aerodynamic noise from high-speed trains, International Journal of Rail Transportation 3(3) (2015) 119-150.
3. C. Talotte, Aerodynamic noise: a critical survey, Journal of Sound and Vibration 231 (3) (2000) 549-562.
4. M.B. Mauclaire, Noise generated by high speed trains: new information acquired by SNCF in the field of acoustics, owing to the high speed test programme, International Conference on Noise Control. Internoise, Gothenburg, 1990.
5. M.A. Pallas, K.P. Schmitz, B. Barsikow, P. Fodiman, G. Holzl, DEUFRAKO: localized sound sources on the high-speed vehicles ICE, TGV-A and TR 07. Internoise, Yokohama, 1994.
6. H. Tsuda, M. Kimata, H. Sawada, Prediction of the Shinkansen noise. in INTER-NOISE and NOISE-CON Congress and Conference Proceedings. Institute of Noise Control Engineering, Internoise, Yokohama, 1994.
7. K. Nagakura, Y. Moritoh, Y. Zenda, Y. Shimizu, Aerodynamic noise of maglev cars. In Inter-Noise and Noise-Con Congress and Conference Proceedings, Institute of Noise Control Engineering, Internoise, Yokohama, 1994.
8. A. Martens, J. Wedemann, N. Meunier, A. Leclere, A.G. Bahn Deutsche, D.B. Systemtechnik, High speed train noise-sound source localization at fast passing trains. Sociedad Espanola de Acoustica, SEA, 2009.
9. N. Curle, The influence of solid boundaries upon aerodynamic sound. Proceedings of the Royal Society of London. Series A. Mathematical and Physical Sciences 231(1187) (1955) 505-514.
10. M.J. Lighthill, On sound generated aerodynamically I. General theory. Proceedings of the Royal Society of London. Series A. Mathematical and Physical Sciences 211(1107) (1952) 564-587.

11. M.E. Goldstein, Aeroacoustics. New York, McGraw-Hill International Book Co., 1976.
12. M. Ikeda, M. Suzuki, and K. Yoshida, Study on optimization of panhead shape possessing low noise and stable aerodynamic characteristics. Quarterly Report of RTRI 47(2) (2006) 72-77.
13. T. Kurita, Y. Wakabayashi, H. Yamada, M. Horiuchi, Reduction of wayside noise from Shinkansen high-speed trains. Journal of Mechanical Systems for Transportation and Logistics 4(1) (2011) 1-12.
14. T. Sueki, M. Ikeda, T. Takaishi, Aerodynamic noise reduction using porous materials and their application to high-speed pantographs. Quarterly Report of RTRI 50(1) (2009) 26-31.
15. T. Mitsumoji, T. Sueki, N. Yamazaki, Y. Sato, M. Ikeda, R. Takinami, H. Gejima, K. Fukagata, Aerodynamic noise reduction of a pantograph panhead by applying a flow control method, in: J.C.O. Nielsen, et al. (Eds) Proceedings of 11th International Workshop on Railway Noise, Uddevalla, Sweden, 9-13 September 2013, Notes on Numerical Fluid Mechanics & Multidisciplinary Design 126 (2015) 515-522.
16. F. R. Grosche, G. Meier, Research at DLR Göttingen on bluff body aerodynamics, drag reduction by wake ventilation and active flow control. Journal of Wind Engineering and Industrial Aerodynamics 89(14-15) (2001) 1201-1218.
17. T. Lölgen, Wind tunnel noise measurements on full-scale pantograph models. The Journal of the Acoustical Society of America (1999) 105:1136.
18. E. Latorre Iglesias, D.J. Thompson, M. Smith, Experimental study of the aerodynamic noise radiated by cylinders with different cross-sections and yaw angles. Journal of Sound and Vibration 361 (2016) 108-129.
19. J.E. Ffowcs Williams, D.L. Hawkings, Sound generation by turbulence and surfaces in arbitrary motion. Philosophical Transactions of the Royal Society of London. Series A, Mathematical and Physical Sciences 264(1151) (1969) 321-342.
20. J. Smagorinsky, General circulation experiments with the primitive equations: I. The basic experiment. Monthly Weather Review 91(3) (1963) 99-164.
21. D.C. Wilcox, Turbulence modeling for CFD. DCW industries La Canada, CA. Vol. 2. 1998.
22. S. Lei, C. Zhang, J. Wang, L. Ren, Numerical analysis of aerodynamic noise of a high-speed pantograph. in Digital Manufacturing and Automation (ICDMA), Fourth International Conference on. IEEE. 2013.
23. H. Kim, Z. Hu, D.J. Thompson, Numerical investigation of the effect of cavity flow on high speed train pantograph aerodynamic noise, Journal of Wind Engineering & Industrial Aerodynamics 201 (2020) 104159.
24. H. Kim, Z. Hu, D.J. Thompson, Effect of cavity flow control on high speed train pantograph and roof aerodynamic noise. Railway Engineering Science 28 (2020) 54-74.
25. H. Kim, Z. Hu, D.J. Thompson, Effect of different typical high speed train recess configurations on aerodynamic noise. Proceedings of the Institution of Mechanical Engineers, Part F: Journal of Rail and Rapid Transit, 235(5) (2021) 573–585.
26. X.W. Liu, Z.W. Hu, D.J. Thompson, V. Jurdic, Reduction of aerodynamic noise from square bars by introducing spanwise waviness. Journal of Sound and Vibration 435 (2018) 323-349.
27. X.W. Liu, D.J. Thompson., Z.W. Hu, V. Jurdic, Numerical investigation of aerodynamic noise generated by circular cylinders in cross-flow at Reynolds numbers in the upper subcritical and critical regimes. International Journal of Aeroacoustics 2019. 18(4-5) 470-495.

28. M. Smith, L. Chow. Prediction method for aerodynamic noise from aircraft landing gear. in 4th AIAA/CEAS Aeroacoustics Conference. 1998.
29. W. Behr, T. Lölgen, W. Baldauf, L. Willenbrink, R. Blaschko, K. Jager, J. Kremlacek, Low noise pantograph ASP recent developments. in internoise 2000. Proceedings of the 29th international congress on noise control engineering, Internoise, Gothenburg, August 2000.
30. E. Latorre Iglesias, D.J. Thompson, M. Smith, Component-based model for aerodynamic noise of high-speed trains, in: J.C.O. Nielsen, et al. (Eds) Proceedings of 11th International Workshop on Railway Noise, Uddevalla, Sweden, 9-13 September 2013, Notes on Numerical Fluid Mechanics & Multidisciplinary Design 126 (2015) 481-488.
31. E. Latorre Iglesias, D.J. Thompson, M. Smith, Component-based model to predict aerodynamic noise from high-speed train pantographs. Journal of Sound and Vibration 394 (2017) 280-305.
32. X. Liu, J. Zhang, D.J. Thompson, E. Latorre Iglesias, G. Squicciarini, Z. Hu, M. Toward, D. Lurcock, Aerodynamic noise of high-speed train pantographs: comparisons between field measurements and an updated component-based prediction model, Applied Acoustics 175 (2021) 107791.
33. J.Q. Guo, J.M. Ge, Z.J. Sun, S.Q. Liu, Y.J. Zhao, J.S. Lin, Pantograph Area Noise and Vibration Transmission Characteristics and Interior Noise Reduction Method of High-Speed Trains. In: Nielsen J. et al. (eds) Noise and Vibration Mitigation for Rail Transportation Systems. Notes on Numerical Fluid Mechanics and Multidisciplinary Design, Berlin, Heidelberg, 126 (2015) 563-570.
34. B. Barhoumi, S.B. Hamouda, J. Bessrour, A simplified two-dimensional boundary element method with arbitrary uniform mean flow, Theoretical and Applied Mechanics Letters 7(4) (2017) 207-221.
35. Z.C. Zheng, W. Li, Numerical stabilities and boundary conditions in time-domain Eulerian simulations of acoustic wave propagations with and without background flow, Applied Mathematics and Computation 202(1) (2008) 146-161.
36. H. Dastourani, I. Bahman-Jahromi, Evaluation of Aeroacoustic Performance of a Helmholtz Resonator System with Different Resonator Cavity Shapes in the Presence of a Grazing Flow, Journal of Aerospace Engineering 34(5) (2021) 04021061.
37. X. Liu, Aerodynamic noise from components of a train pantograph and its reduction. PhD Thesis, the University of Southampton, 2017.
38. H. Li, D.J. Thompson, G. Squicciarini, Using a 2.5D boundary element method to predict the noise on the train side due to rolling noise. Journal of Sound and Vibration 486 (2020) 115599.
39. D. Duhamel, Efficient calculation of the three-dimensional sound pressure field around a noise barrier. Journal of Sound and Vibration 197(5) (1996) 547-571.
40. Y. Zhang, J. Zhang, T. Li, L. Zhang, Investigation of the aeroacoustic behavior and aerodynamic noise of a high-speed train pantograph. Science China Technological Sciences 60(4) (2017) 561-575.
41. H.A. Schenck, Improved integral formulation for acoustic radiation problems. The Journal of the Acoustical Society of America 44(1) (1968) 41-58.
42. X. Zhang, D.J. Thompson, H. Jeong, G. Squicciarini, The effects of ballast on the sound radiation from railway track. Journal of Sound and Vibration 399 (2017) 137-150.
43. C. Baker, T. Johnson, D. Flynn, H. Hemida, A. Quinn, D. Soper, M. Sterling, Train aerodynamics: fundamentals and applications, Butterworth-Heinemann, Oxford, 2019.
44. C. Bailly, G. Comte-Bellot, Wall-Bounded Turbulent Flows in Turbulence. Springer. 2015.

45. COMSOL Manual, Introduction to the Acoustics Module, version 5.6.
46. F.Q. Hu, On absorbing boundary conditions for linearized Euler equations by a perfectly matched layer, Journal of Computational Physics 129(1) (1996) 201-219.
47. A.D. Pierce, R.T. Beyer, Acoustics: An introduction to its physical principles and applications. Acoustical Society of America, 1990.